JOURNAL OF MATERIALS SCIENCE 29 (1994) 6439–6444

Production of SiC particulate reinforced aluminium composites by melt spinning

N. J. FEI, L. KATGERMAN, W. H. KOOL
Delft University of Technology, Laboratory of Materials Science and Technology, Rotterdamseweg 137, 2628 AL Delft, The Netherlands

Melt spinning is successfully used for the preparation of a rapidly solidified SiC particle reinforced AlSi7Mg0.3 alloy. The composites are prepared by introducing SiC particles in a semi-solid matrix slurry (SiC volume fractions up to 0.15, particle size 10 or 20 μm). Duralcan material (SiC volume fraction 0.20, particle size 12 μm) was also used. After stirring in the semi-solid state the composites are heated above the liquidus temperature and subsequently melt-spun. Featureless, columnar and dendritic zones can be identified in the ribbons. A finer dendritic structure is found around the SiC particles. The SiC particles tend to segregate to the air side of the ribbons and the segregation effect is influenced by particle size and volume fraction. As interface velocities are higher than the critical velocities predicted by models on interface pushing, it is concluded that fluid flow in the melt puddle is responsible for the segregation effect.

1. Introduction

Development of advanced materials for high-performance applications involves both design of new materials and application of new processing techniques. During the last decades increasing attention has been paid to metal matrix composites (MMCs) because of their attractive properties. The introduction of a ceramic phase plays an important role in improving various properties such as strength, stiffness and wear resistance. Both powder and ingot metallurgy are widely used for the preparation of MMCs, and each has disadvantages. Powder metallurgy is a multi-step process, resulting in high materials costs. It also encompasses the handling of fine powder, which involves severe risks. Ingot metallurgy is cost-effective, but microstructures are coarser and segregation effects and poor particle distribution may occur.

Rapid solidification processing has attracted widespread interest for the development of various materials. Because of the high cooling rates the materials have refined microstructure, improved compositional uniformity and a high level of supersaturation. Mechanical properties and especially ductility are improved.

The application of melt spinning for the fabrication of composites has been the subject of several studies [1–6]. For aluminium MMCs it is reported that rapid solidification results in a strong improvement in elongation compared to conventional processing [1, 2], and notification has been made of local agglomeration of particulates [3–5] or particle segregation effects [1, 6] in the ribbons.

In general, the distribution of a reinforcement phase in composites prepared by ingot metallurgy is determined by the behaviour of particles in front of a moving solid/liquid interface, at which they are either pushed, engulfed or entrapped. This behaviour has been the subject of several studies [7–11]. In determining whether the ceramic particles are pushed or engulfed by an advancing solidification front, many variables such as growth velocity of the solid phase, particle surface energy, particle size and shape, volume fraction of particles both in the material and at the interface, temperature gradient ahead of the interface, viscosity of the liquid and solid/liquid interface shape must be considered. Particle pushing is promoted by decreasing particle size, lower particle concentration and lower melt viscosity.

The aim of this study is to prepare MMCs by melt spinning and to investigate the influence of rapid solidification processing on the microstructure and the particle distribution in the ribbons. In order to avoid chemical reactions in the long contact period between SiC and the liquid aluminium alloy during compocasting, a matrix alloy of relatively high Si content is used. Optical microscopy revealed that indeed no reaction products between aluminium and SiC are present in these composites [6]. The paper discusses whether the above-mentioned models of pushing/engulfment of particles at the solid/liquid interface are adequate to predict the present results on particle distribution at high interface velocities.

2. Materials and methods

Aluminium composites were prepared by compocasting and subsequently melt-spun. The casting alloy A356 (AlSi7Mg0.3) was used as the matrix alloy. SiC particulates of 10, 20 or 23 μm average diameter with

0022–2461

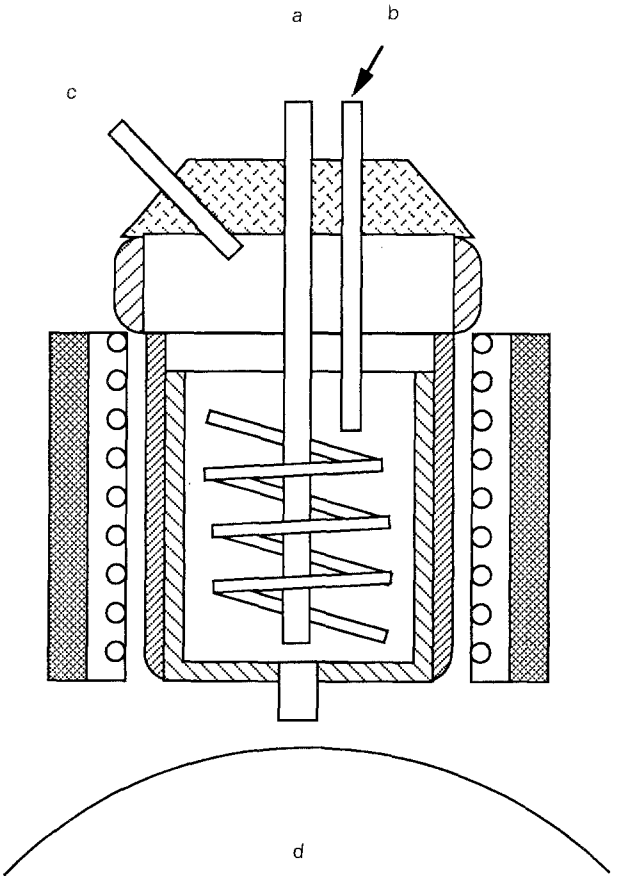

Figure 1 Production unit. (a) Stirrer; (b) SiC addition; (c) argon supply and (d) spinning wheel.

volume fractions up to 0.15 were introduced. The equipment used for the preparation is shown in Fig. 1. It consists of a graphite crucible which contains the slurry and is located in an electrical resistance furnace. A stirrer with spirally shaped blades was used to shear the slurry and provide efficient mixing of SiC with the aluminium alloy. After the temperature of the matrix alloy reached the intended value in the semi-solid state regime, SiC particles were introduced. Then the composite slurry was further stirred at the same temperature for about 1 h to obtain homogeneous distribution and to promote wetting of the SiC particles. Then the slurry was remelted and the composite melt was ejected at 750 °C with an ejection pressure of 20 mbar. The ejection took place through a 1.5 mm circular orifice on a copper wheel, rotating with a circumferential velocity of about 20 $m\,s^{-1}$. The distance between orifice and wheel was 6 ± 1 mm. During the processing argon gas was used for protection against oxidation. In addition, Duralcan F3A20S (matrix: A356; SiC particles: 20 vol%, 12 μm average diameter) was also melt-spun.

3. Results

3.1. Matrix ribbons

A typical matrix ribbon microstructure is shown in Fig. 2. Three regions are distinguished in the ribbon from wheel side to upper side. A featureless zone is visible at the wheel side. This is free of segregation as a result of the diffusionless solidification in this zone due to the extremely high cooling rate. A columnar zone is present in the middle of the ribbons: the columns are found to be nearly perpendicular to the spinning direction. An equiaxed dendritic zone is located at the air side. The microstructure in this region is coarser than in the featureless or columnar zone: the average grain size is about 2 μm.

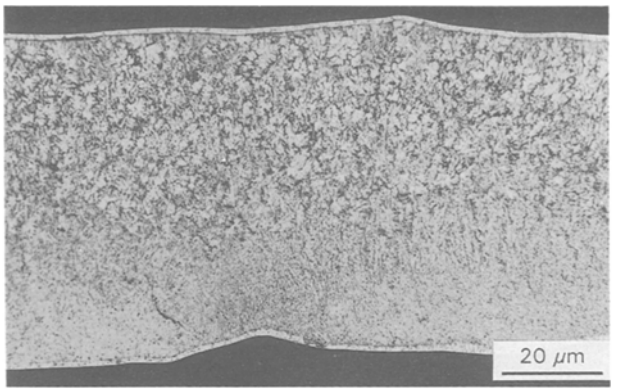

Figure 2 Optical micrograph showing the microstructure of the matrix alloy ribbon. Top: air side; bottom: wheel side.

3.2. Composite ribbons

3.2.1. Production aspects

Composites containing 10, 20 or 23 μm SiC particles with particle concentrations up to 15 vol% were successfully prepared by compocasting and melt-spinning. In addition, Duralcan composites were melt-spun with particle concentrations around 17 vol%. Compared to matrix alloys, the same melt-spinning parameters such as ejection pressure, orifice diameter and wheel speed could be used for the production of composite ribbons. The surface of the ribbons at the wheel side is much smoother and more shiny than at the air side. The surface of composites at the air side becomes dimmer with increasing SiC content. The SiC concentrations in the composite ribbons, determined by CO_2 analysis after oxidation in O_2 (Ströhlein CS-mat 650 equipment), are listed in Table I. For the composites reinforced with 20 or 23 μm particles, the actual SiC concentrations in the ribbons are not much different from the nominal

TABLE I SiC particle concentration in the composite ribbons

Composite batch	SiC size (μm)	Volume concentration	
		nominal (%)	actual (%)
1	20	5	4
2	20	10	8
3	20	15	13
4	10	5	3
5	10	10	8
6	10	15	10
7	12	20	17
8	23	17	15

concentrations. For the 10 μm particles, the difference between nominal and actual concentrations becomes larger. The differences found are ascribed to some loss of particles during the introduction stage as well as to incomplete ejection of the composite melt from the crucible, which leaves behind a higher concentrated part in the crucible.

3.2.2. Ribbon morphology

The width of all ribbons is about 2–2.5 mm. Their thickness measured by a micrometer gauge varies from 80 to 140 μm and is independent of particle concentration. This thickness is higher than the actual average thickness because of surface roughness, which increases strongly with increasing particle concentration (Fig. 3). Using optical microscopy, the roughness value is determined by taking the ratio of the difference of greatest and smallest thickness, and the average thickness. It is further found that the roughness becomes less for smaller particles.

3.2.3. Microstructure

The distribution of 20 μm SiC particles in the composite ribbon is shown in Fig. 4. There is a strong tendency for the SiC particles to segregate to the upper part of the ribbon. In the ribbons with lower volume fractions of SiC, most particles are located at the air side, whereas only a few are found at the wheel side. With increasing SiC content (Fig. 4c) many more particles are observed at the wheel side although a majority is still found at the air side. A zone depleted of particles is present in the central part of the ribbon. Similar effects of particle distribution are observed in the composites with 10 μm SiC particles, as shown in Fig. 5. However, for the smaller particle size, many more SiC particles are detected at the wheel side of the ribbons and a few are observed in the middle. Fig. 6 demonstrates that segregation also takes place in ribbons prepared from Duralcan material. Apart from the segregation effect, significant variations in average SiC content are observed along the longitudinal direction of the ribbons, probably due to non-uniform distributions in the melt. It is noted that the SiC

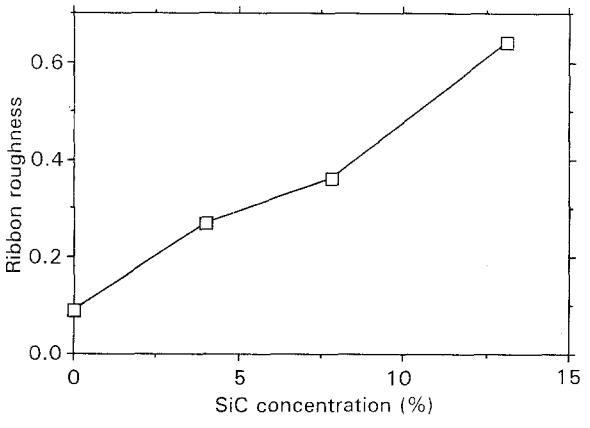

Figure 3 Ribbon roughness versus SiC (20 μm) particle concentration.

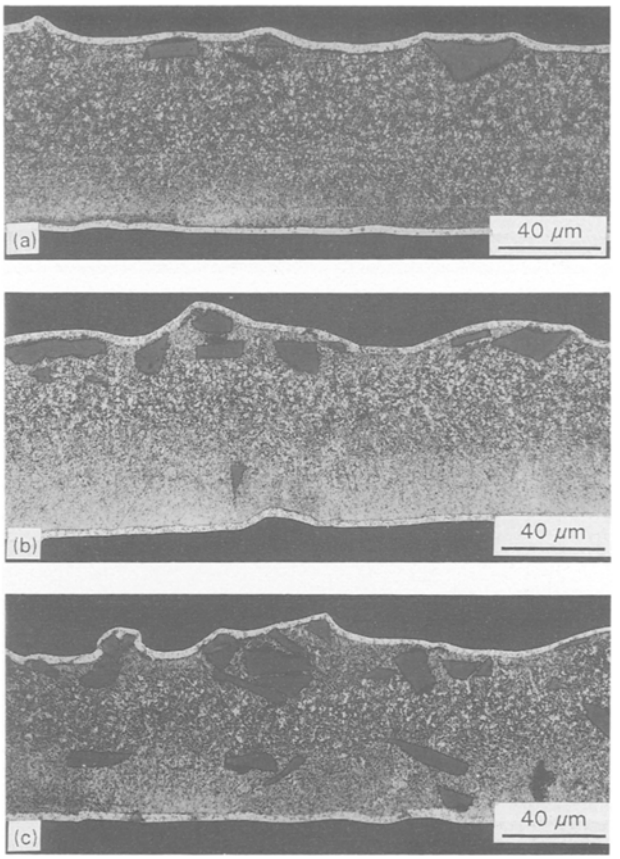

Figure 4 Optical micrographs of composite ribbons with 20 μm SiC particles. (a) 5 vol%, (b) 10 vol%, (c) 15 vol%. Section taken along longitudinal direction. Top: air side; bottom: wheel side.

particles in the ribbons are well wetted by the matrix alloy as the SiC particles near the top surface of the ribbons are always covered by a thin layer of the aluminium alloy. It is also observed that, at the air side of the ribbon, the main axis of acicular particles tends to become parallel to the surface of the ribbons. The main axes of acicular particles near the wheel side are randomly distributed.

In order to quantify the SiC particle distribution in the ribbon, it was divided into three regions of equal thickness (air side, central part and wheel side). The ratios N_b/N_t and N_m/N_t were determined, indicating the ratio of the number of particles at the wheel side and the air side and the ratio of the number of particles in the central part and at air side respectively. These ratios are shown in Fig. 7. It is seen that with decreasing SiC content N_b/N_t as well as N_m/N_t decrease, implying a more pronounced segregation effect. N_b/N_t is always higher than N_m/N_t, implying a certain retention of SiC particles at the wheel side of the ribbon. N_b/N_t and N_m/N_t are lower for 20 μm particles resulting in a more pronounced segregation effect for bigger particles.

In the composite ribbons the featureless, columnar and dendritic zones can be distinguished similarly to those in the matrix ribbons. However, with the addition of SiC, the dendritic zone in the ribbons becomes larger, due to the lower thermal conductivity. In the upper part of the ribbon, the equiaxed dendrites are slightly smaller near the SiC particles, which indicates

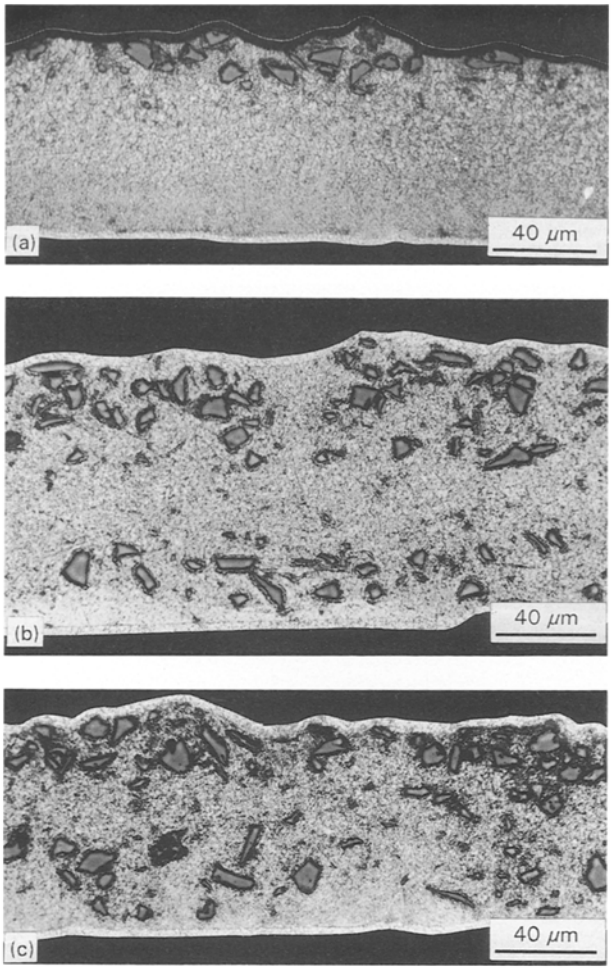

Figure 5 Optical micrographs of composite ribbons with 10 μm SiC particles. (a) 5 vol%, (b) 10 vol%, (c) 15 vol%. Section taken along longitudinal direction. Top: air side; bottom: wheel side.

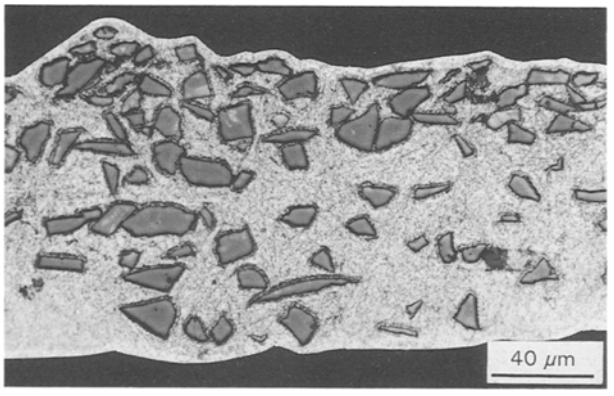

Figure 6 Optical micrograph showing distribution of 12 μm SiC particles in the ribbons, prepared from Duralcan material. Top: air side; bottom: wheel side.

TABLE II Secondary dendrite arm spacing (DAS) and local ribbon thickness. SiC size is 20 μm

SiC concentration (%)	DAS middle (μm)	DAS air side (μm)	Local thickness (μm)
0	0.59	0.69	49.7
4	0.61	0.67	71.4
8	0.75		54.1
13	0.79		44.3

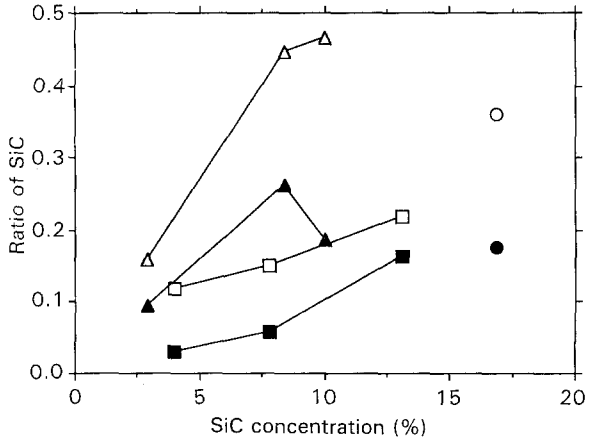

Figure 7 Ratios N_b/N_t ((△): 10 μm; (□): 20 μm; (○): Duralcan) and N_m/N_t ((▲): 10 μm; (■): 20 μm; (●): Duralcan) versus SiC content. Ratios equal to 0 and 1 correspond to complete segregation and absence of segregation respectively.

that the presence of SiC particles promotes nucleation. In Table II the results of dendrite arm spacing (DAS) measurements is given for the matrix alloy and for the composites with 20 μm particles. DAS increases with particle concentration.

4. Discussion

4.1. Production aspects

Rapidly solidified ribbons were obtained containing maximum concentrations of 15–17 vol% after introducing 20 μm particles or using Duralcan material and 10 vol% after introducing 10 μm particles. Particle loss occurs during the introduction stage and during ejection when particles will stick to the crucible wall. The loss of smaller particles is more severe due to the larger specific surface area in combination with the low wettability which results in stronger particle segregation. The limitations in particle concentration have been reported earlier [1, 2].

4.2. Calculation of interface velocity and critical velocity of particle pushing

In order to discuss the particle segregation effect observed in the ribbons in the framework of the theories of particle pushing, the interface velocities during solidification of the ribbons have to be determined. First we calculate the cooling rate from the DAS values, given in Table II. Their relation is given in power law form by several authors [12–15] with various constants and exponents. In the regime of our interest, values for the cooling rate may vary by a factor as large as 25. An expression, put forward in [14], accounts for a reasonable melt length outside the puddle and is given by

$$\mathrm{DAS} = 47\left(\frac{\mathrm{d}T}{\mathrm{d}t}\right)^{-0.33} \quad (1)$$

where DAS is the secondary dendrite arm spacing (μm) and $\mathrm{d}T/\mathrm{d}t$ is the cooling rate ($\mathrm{K\,s^{-1}}$). With the assumption of Newtonian cooling the heat-transfer

coefficient h is calculated from the cooling rate using

$$h = \frac{\rho_{Al} C_p d}{T - T_w} \cdot \frac{dT}{dt} \quad (2)$$

where ρ_{Al}, C_p, d, T and T_w are liquid density, specific heat, ribbon thickness, melt temperature and wheel temperature respectively [16]. The interface velocity is then calculated using the relation.

$$V = \frac{h(T - T_w)}{\rho_{Al} \Delta H} \quad (3)$$

where V and ΔH are interface velocity and latent heat of fusion respectively [16]. Values for cooling rate, heat transfer coefficient and interface velocity are presented in Table III. Interface velocities range from 30 to 90 mm s^{-1}.

The theory of particle pushing as put forward by Stefanescu *et al.* [7–10] accounts for two forces acting on a particle in the vicinity of a solidification front, i.e. the pushing force and the drag force arising from a difference in surface energy and particle movement in a viscous medium respectively. A critical velocity of the interface V_{cr} is defined beyond which interface pushing is prohibited. Due to the non-steady-state conditions during solidification in the puddle we assume the interface in the immediate vicinity of the particle to be planar and not disturbed by local thermal effects. The critical velocity of the interface is then given by [7, 8]

$$V_{cr} = \frac{\Delta\sigma_0 2a_0}{3(n-1)\eta d} \quad (4)$$

in which $\Delta\sigma_0$, $2a_0$, n, η and d are difference in surface tension, interatomic distance, value of the exponent describing the decrease of the surface tension versus distance, melt viscosity and particle diameter respectively. V_{cr} is plotted against particle diameter in Fig. 8 using the values given in Refs 7 and 8. Modified formulae are given in more recent work [9, 10] but these lead to much lower values of V_{cr}. These results are also included in Fig. 8. It is clear that much uncertainty exists in the calculations as several thermophysical properties are not precisely known.

TABLE III Cooling rate, heat transfer coefficient and interface velocity, calculated from dendrite arm spacing values

SiC concentration (%)	Cooling rate (10^5 °C s^{-1})	h (10^4 J m^{-2} s^{-1} K^{-1})	V (mm s^{-1})
0	5.77	8.54	66
4	5.22	1.09	89
8	2.79	0.44	38
13	2.38	0.30	27

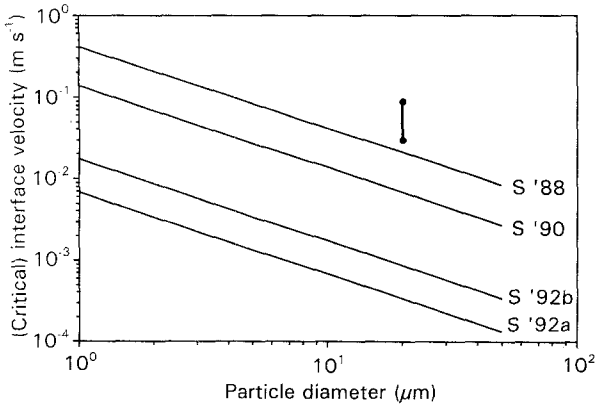

Figure 8 Critical interface velocity versus particle diameter. S'88, S'90, S'92a and S'92b refer to Refs 7–10 respectively. (●) Interface velocities, calculated from dendrite arm spacing values.

4.3. Comparison of interface velocity and critical velocity

From Fig. 8 it appears that interface velocities during rapid solidification are higher than the critical velocities predicted for interface pushing. This should lead to particle engulfment and not to segregation, which is in contradiction to the experimental observations. Also, critical velocities are higher for particles of smaller diameter, which implies that smaller particles are more easily pushed. In contrast, from Fig. 7 it appears that for SiC concentrations in excess of ~ 2.5 wt % the larger particles segregate more strongly. However, the particle segregation for concentrations close to zero tends to be nearly complete for both particle diameters. For these low concentrations, for which in fact Equation (4) was derived, it cannot be decided whether or how particle diameter influences the tendency to segregation.

It is concluded that the observed segregation effect is not explained by particle pushing alone. Another effect has to be taken into account. A probable explanation is that, whereas interface velocities are around 30–90 mm s^{-1}, flow velocities in the melt puddle, which are nearly parallel to the interface, are around 25 m s^{-1}. Current particle pushing models should be extended by taking into account the convective motion of particles in the puddle.

5. Conclusions

1. Melt spinning can be used successfully for the preparation of rapidly solidified aluminium metal matrix composites, reinforced by SiC particles. Average SiC diameters were from 10 to 23 μm and volume fractions were up to 0.17.

2. Featureless, columnar and dendritic zones are identified in the ribbons. The dendritic zone is larger for the composite, due to the lower cooling rate. A finer microstructure around SiC particles is found, due to enhanced nucleation.

3. SiC particle distribution in the ribbons is inhomogeneous over the thickness of the ribbon, and they tend to segregate to the air side. Large particles segregate more strongly than small particles. With increasing volume fraction of SiC, SiC particle distribution becomes more homogeneous.

4. Existing models of particle pushing do not predict this segregation effect. The fluid dynamics in the melt puddle has to be taken into account.

Acknowledgements

The authors thank H. Kleinjan for his helpful contributions and P. de Ruiter for his skilful assistance during preparation of the composite ribbons.

References

1. J. C. EHRSTRÖM and W. H. KOOL, *J. Mater. Sci.* **23** (1988) 3195.
2. W. R. LOUÉ and W. H. KOOL, in Proceedings of International Symposium on Advances in Cast Reinforced Metal Composites, Chicago, 1988, edited by S. G. Fishman and A. K. Dhingra (American Society for Metals, Metals Park, OH, 1988) p. 327.
3. P. G. ZIELINSKI and D. G. AST, *J. Mater. Sci. Lett.* **2** (1983) 495.
4. *Idem*, in Proceedings of MRS Symposium on Rapidly Solidified Metastable Materials, Boston, USA, 1983, edited by B. H. Kear and B. C. Giessen (Elsevier, New York, 1984) p. 189.
5. *Idem, Scripta Metall.* **17** (1983) 291.
6. N. J. FEI and W. H. KOOL, in Proceedings of International Conference on Metal Matrix Composites III: Exploiting the Investment, Dec. 10–11, 1991, London, UK (Institute of Metals, London, 1991) p. 1/P1.
7. D. M. STEFANESCU, B. K. DHINDAW, S. A. KACAR and A. MOITRA, *Metall. Trans.* **A19** (1988) 2847.
8. D. M. STEFANESCU, A. MOITRA, A. S. KACAR and B. K. DHINDAW, *ibid.* **A21** (1990) 231.
9. D. SHANGGUAN, S. AHUJA and D. M. STEFANESCU, *ibid.* **A23** (1992) 669.
10. D. M. STEFANESCU, S. AHUJA, B. K. DHINDAW and R. PHALNIKAR, in Proceedings of IInd International Conference on Processing of Semi-Solid Alloys and Composites, Cambridge, MA, USA, 1992, edited by S. B. Brown and M. C. Flemings (TMS Publ. 472) p. 406.
11. A. R. KENNEDY and T. W. CLYNE, *Cast Metals* **4** (1991) 160.
12. R. E. SPEAR and G. R. GARDNER, *Trans. Am. Foundry Soc.* **71** (1963) 209.
13. T. F. BOWER, H. D. BRODY and M. C. FLEMINGS, *Trans. Met. Soc. AIME* **236** (1966) 624.
14. G. R. ARMSTRONG and H. JONES, in Proceedings of International Conference on Solidification and Casting of Metals, Sheffield, UK, 1977 (The Metals Society, London, 1979) p. 454.
15. M. BAMBERGER, B. Z. WEISS and M. M. STUPEL, *Mater. Sci. Techn.* **3** (1987) 49.
16. H. JONES, in "Rapid Solidification of Metals and Alloys" (The Institution of Metallurgists, London, UK, 1982).

Received 16 December 1993
and accepted 27 May 1994